Magnetotransport in Nonplanar SiGe/Si Nanomembranes

Gregory J. Meyer, Neville L. Dias, Robert H. Blick, and Irena Knezevic, *Member, IEEE*

***Abstract*—We investigate the relationship between electronics and geometry in a nonplanar SiGe/Si resonant quantum cavity (RQC) subject to a magnetic field. The transfer matrix technique originally due to Usuki *et al.* [*Phys. Rev. B*, vol. 52, pp. 8244–8255, 1995] has been modified to account for the nonzero local curvature of the RQC. Our results demonstrate that low-temperature ballistic magnetoconductance in nonplanar RQCs is highly sensitive to the changes in curvature for a wide range of magnetic field strengths.**

***Index Terms*—Curved nanostructures, geometric potential, magnetotransport, Si/SiGe nanomembranes.**

I. Introduction

RECENT interest in nonplanar 2-D (NP2D) electron systems [1] has been driven by the emergence of reliable techniques for fabrication of flexible heterostructures, based on strained Si/SiGe [2]–[4] or GaAs [5], [6]. Curvature has become another degree of freedom available for manipulating electronic systems, which leads to novel basic physics and suggests applications of NP2D systems in nanoelectromechanical systems (NEMS) as ultrasensitive scales and sensors. The ability to design quantum devices using flexible substrates increases with our understanding of the role played by geometry in determining the electrical properties of these systems [7]–[10]. Therefore, there is a need for versatile modeling tools capable of capturing the physics in nonplanar structures in a variety of geometries, biasing regimes, temperatures, and magnetic fields. To that end, we have made modifications to a transfer-matrix technique [11], [12], widely and successfully implemented at low magnetic fields and in planar 2-D systems [13]–[15], in order to expand its functionality to include magnetic fields in nonplanar geometries.

In this paper, we present a calculation of low-temperature ballistic magnetoconductance in a nonplanar resonant quantum cavity (RQC) under low bias, based on the modified transfer-matrix method. The simulated 300 × 300 nm^2 RQC (Fig. 1) is formed on a ⟨100⟩ SiGe/Si heterostructure upon selective etching of the sacrificial oxide layer under the cavity's wings. Narrow (50 nm) quantum-point contacts connect the cavity to the wide leads (not depicted) at the source and drain ends; the rigid leads and the cavity spine are flat and tethered to the substrate. The 2-D electron system is formed at the interface between the undoped strained Si and the relaxed, phosphorous-doped SiGe underneath (for example, epitaxially grown on SOI [4]). The structure can be topped with another layer of n-type doped SiGe to aid in the electronic confinement [4]; such SiGe/Si modulation doped heterostructures have been shown to produce good electronic confinement both before and after selective etching of the sacrificial oxide layer. But unlike the strain-compensated structure of [4] that remained flat upon underetching, our structure releases the wings to curl up into a partial cylinder, similar to what happens in the inverted Si/SiGe structure described in [3] that curled downward. Curvature is measured in terms of a parameter $\alpha = W/(\pi R)$, where W is the width of the cavity, and R is the radius of curvature.

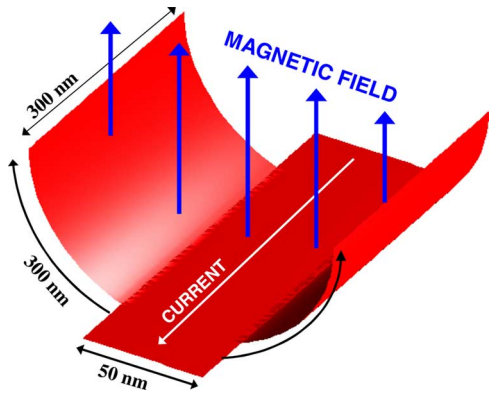

Fig. 1. A nonplanar resonant quantum cavity on a SiGe/Si heterofilm, formed by selective etching of the sacrificial layer under the cavity's wings. Strain from the lattice mismatch provides the force that causes the wings to bow. Curvature is measured terms of $\alpha = W/(\pi R)$, where W is the width of the cavity and R is the radius of curvature.

In Section II, we introduce the modified transfer-matrix method, applicable for low-bias transport in nonplanar structures under magnetic field. Simulation results illustrating the effects of curvature on transport are presented in Section III, and concluding remarks are given in Section IV.

II. The Modified Transfer-Matrix Method

The transfer-matrix method due to Usuki *et al.* [11] is an iterative, stable routine used to solve the discretized 2-D Schrödinger equation. The entire numerical domain is divided into slices perpendicular to the current flow. A transfer matrix is constructed for each slice and, after iterating slice-by-slice in the direction of the current flow, the space-resolved electron density and the

Manuscript received June 10, 2006; revised March 8, 2007. This work was supported by the National Science Foundation through the University of Wisconsin MRSEC and Award ECCS-0547415. The review of this paper was arranged by Associate Editor R. Lake.

The authors are with the Department of Electrical and Computer Engineering, University of Wisconsin-Madison, Madison, WI 53706 USA (e-mail: knezevic@engr.wisc.edu).

Color versions of one or more of the figures in this paper are available online at http://ieeexplore.ieee.org.

Digital Object Identifier 10.1109/TNANO.2007.896848

structure's transmission coefficient are obtained. In the absence of a magnetic field

$$\begin{bmatrix} \psi_n \\ \psi_{n+1} \end{bmatrix} = T_n \begin{bmatrix} \psi_{n-1} \\ \psi_n \end{bmatrix},$$
$$T_n = \begin{bmatrix} \hat{0} & \hat{I} \\ -\hat{H}_{n,n+1}^{-1}\hat{H}_{n,n-1} & \hat{H}_{n,n+1}^{-1}(E\hat{I} - \hat{H}_n) \end{bmatrix},$$
$$\hat{H}_{n,n+1} = \hat{H}_{n,n-1} = \mathrm{diag}[-E_0] \quad (1)$$

where ψ_n is the wavefunction of the n-th slice, T_n is the transfer matrix from slice $n-1$ to slice n, $\hat{H}_{n,n\pm1}$ are the hopping Hamiltonian matrices that connect nearest-neighbor slices, and $\hat{H}_n$ is the finite-difference representation of the Hamiltonian of the n-th slice. All these Hamiltonians are matrices of dimension M, where M is the number of gridpoints in the direction perpendicular to the current flow, while ψ_n is an M-column. Moreover, $E_0 = \hbar^2/2m^*a^2$ is the nearest-neighbor hopping energy, where a is the mesh spacing (assumed constant throughout the structure), and m^* is the electron effective mass. Since Si is biaxially strained in a {100} plane, among its six equivalent valleys the two whose heavy mass is along the growth direction come down in energy with respect to the other four (the so-called valley splitting into two lower Δ_2 and four higher Δ_4 valleys [16]). The electrons in Δ_2 valleys respond to in-plane bias with the light mass $m^* = 0.19m_0$ (m_0 is the free-electron rest mass), which is the effective mass we use in the calculation. The subbands emerging from the Δ_2 valleys upon confinement are considered twofold degenerate (although the magnetic field can introduce further splitting [16]). We will assume that only the lowest (twofold degenerate) Δ_2 subband is occupied. The total electron sheet density in the leads, $2N$, and the Fermi level E_F measured with respect to the subband bottom are therefore connected by

$$N = \frac{m^*E_F}{\pi\hbar^2}. \quad (2)$$

In order to calculate conductance though the structure, the transmission coefficient for each propagating mode injected from the source is calculated. At the source end of the device, there is a wide lead (not depicted in Fig. 1), where many plane waves are injected with unit amplitude into the device's active region (cavity plus quantum-point contacts); only some make it all the way through to the drain lead, with their amplitude significantly diminished. Plane wave injection at the source end is achieved by solving (1) for $n = 0$ and $\psi_1 = \psi_0 e^{ika}$ (phase shift between two adjacent slices will be ka when a plane wave is injected, where k is the wave number), so

$$e^{ika}\begin{bmatrix} \psi_0 \\ \psi_1 \end{bmatrix} = T_0 \begin{bmatrix} \psi_0 \\ \psi_1 \end{bmatrix}. \quad (3)$$

Since the elements of the transfer matrix T_0 are real [(1)] in the absence of magnetic field, the forward and backward propagating modes occur in pairs: of the $2M$ modes obtained, M are forward and M are backward modes; for each direction, a small number of those M modes are propagating and the rest are evanescent, and the latter do not contribute to the conductance. Only the forward propagating modes enter into the conductance calculations, and thus must be selected from the collection of e^{ika} eigenvalues. This is a straightforward process in the absence of magnetic field: all propagating modes will have real k values, and can be identified as $|e^{ika}| = 1$. Forward modes will have positive k values, and thus $\mathrm{imag}(e^{ika}) > 0$. Note that the grid spacing a must be sufficiently small to ensure that all $ka < \pi$.

A. Modifications for Magnetic Fields

In the presence of a magnetic field, a gauge-invariant form of the Schrödinger equation with the magnetic field incorporated can be obtained through the Peierls substitution [17]. This substitution has the effect of producing the $(\vec{p} + e\vec{A})^2$ term in the full Hamiltonian, which in itself is not suitable for implementation in transfer-matrix approaches.

At zero magnetic field, one can obtain the matrix elements H_{pq} of a tight-binding Hamiltonian by discretizing the Schrödinger equation. The effect of the magnetic field is introduced by modifying each Hamiltonian matrix element H_{pq} by an appropriate Peierls phase factor, containing the integral of the magnetic vector potential along a straight line connecting meshpoints p and q [18]–[20]

$$H_{pq} \to H_{pq}\left(\frac{ie}{\hbar}\int_p^q \vec{A}\cdot d\vec{\ell}\right). \quad (4)$$

In the Landau gauge $\vec{A} = (-By, 0, 0)$, the presence of the magnetic field in the transfer matrix method is felt only in $\hat{H}_{n\pm1}$

$$(\hat{H}_{n,n+1})_{jj} = -E_0 \exp(i2\pi j\Phi/\Phi_0), \quad j = 1, \ldots, M,$$
$$\hat{H}_{n,n-1} = \hat{H}_{n,n+1}^{\dagger} \quad (5)$$

where $\Phi = Ba^2$ is the flux through a meshcell, and Φ_0 is the magnetic flux quantum.

When the magnetic field is present, the matrix elements of T_0 become complex, and the forward and backward propagating modes are no longer mutual complex conjugates. Since the essence of the transfer-matrix technique is proper initialization of forward propagating modes, the selection process becomes more complicated. Namely, the eigenvalues $\exp(ika)$ the phase shifts associated with the modes all get an extra positive phase shift proportional to Φ/Φ_0, which is roughly an average of all the Peierls' phases within one slice [12]. Consequently, some modes that are actually backward propagating may erroneously be identified as forward propagating (see the middle panel of Fig. 2). With increasing magnetic field, one can always first try to decrease a, the meshsize, to minimize the phase shift, but one quickly runs into problems with computer memory (number of meshpoints in the structure and consequently the dimensions of matrices dealt with become too large). Instead, we have found that a simple shift of the coordinate origin—placing the origin at the center of the slice rather than the edge (Fig. 2)—keeps this extra phase shift virtually negligible up to very high magnetic fields. Certainly, this is not a fundamental physical issue, but rather a particularity of the transfer matrix technique.

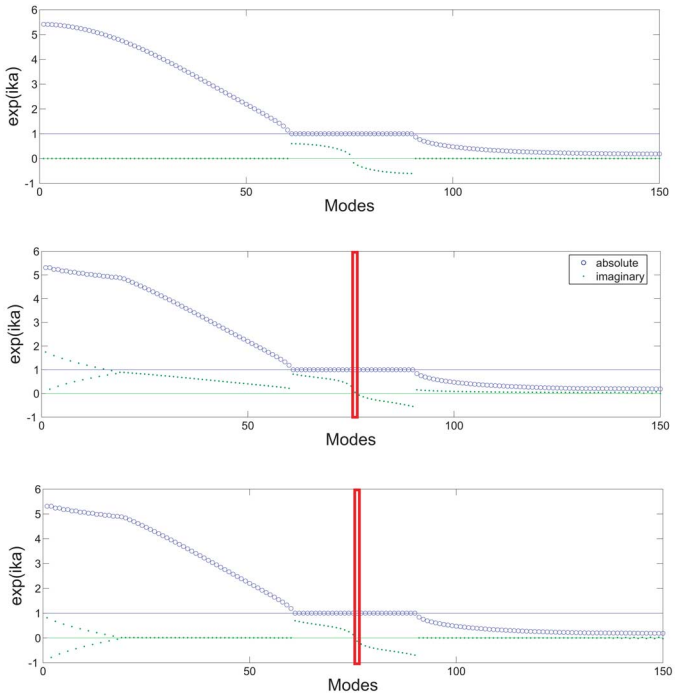

Fig. 2. Absolute values and imaginary parts of all modes for a 300 nm wire at $N = 4 \times 10^{11}$ cm^{-2} and $B = 0$ (top graph) and $B = 0.4$ T (middle and bottom graphs). The Peierls phase skews the imaginary values of all eigenvalues and erroneously reports an extra forward propagating mode (red box) under this moderate magnetic field (middle graph). This skewing effect is eliminated by taking $\int \vec{A} \cdot d\vec{\ell}$ from the center of each stage (bottom graph) rather than the edge.

B. Modifications for Nonplanar Geometries

To investigate the effects of curvature combined with the presence of a magnetic field, the transfer matrix implementation must be further modified.

In the absence of a magnetic field, the motion of a particle confined to a curved surface can be described in the surface's natural coordinates, but with the addition of an extra attractive geometric potential [21]. The geometric potential V_g depends on the mean and Gaussian curvatures of the surface at a given point. For example, in the case of a cylindrical surface of radius R, the geometric potential is a constant and is given by $V_g = -\hbar^2/8m^*R^2$. Indeed, the transfer matrix method as described in Section II is perfectly applicable to other geometries, provided that one accounts for V_g, obeys the structure's modified metric when constructing the kinetic energy operator (details can be found in DaCosta [21]), and discretizes the Schrödinger equation in the surface's natural coordinates.

When a magnetic field is added to the motion over a nonplanar surface, the line integral $\int \vec{A} \cdot d\vec{\ell}$ that is used in modifying the Hamiltonian matrix elements H_{pq} must now be taken *over a geodesic between p and q* rather than along a straight line. This implies that one first needs to calculate the equations for the geodesics for the surface, and then integrate over those to obtain the Peierls phase.

III. Results

The aforementioned modifications were made to the transfer matrix method in order to observe the effects of curvature on the electronic properties of the nonplanar RQC depicted in Fig. 1. Our system is not fully cylindrical (it has cylindrical wings and a flat spine) and is therefore more complicated than a cylinder due to the varying geometric potential: V_g is constant and attractive in the wings, and zero in the spine. (An interested reader can find the analytical solution to magnetotransport on a cylinder with very small curvature in [5].)

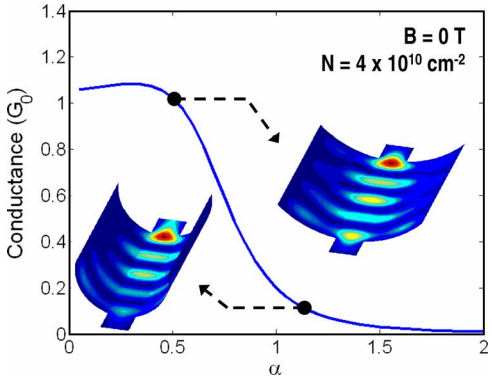

Fig. 3. Conductance variation with curvature at $B = 0$. At particular electron densities in the leads, the conductance is highly dependent on the curvature of the cavity even in the absence of a magnetic field. This phenomenon can only be attributed to the geometric potential. Insets: colorized plots of the magnitude squared of the wavefunction at the Fermi energy, for the specific values of α shown.

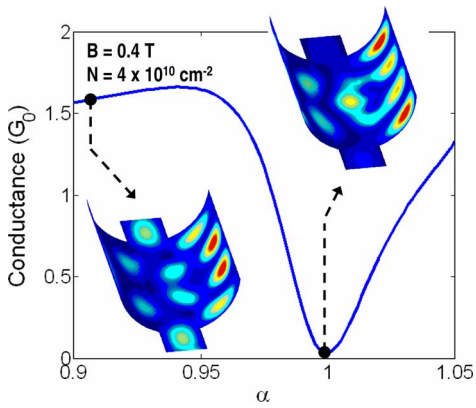

Fig. 4. Conductance variation with curvature at a low magnetic field ($B = 0.4$ T). Insets: colorized plots of the magnitude squared of the wavefunction at the Fermi energy, for the specific values of α shown. Patterns observed in the probability density are altered by changes in curvature, significantly affecting the conductance.

In Figs. 3–6, conductance variations in the structure (in units of $G_0 = 2e^2/h$, the conductance quantum) are presented. All the results are obtained in the low-bias regime as well as at low temperatures, so the electron transport occurs at the Fermi level, specified by N, the electron sheet density (per Δ_2 valley) in the source and drain leads [(2)]. Conductance calculated is also per Δ_2 valley. Conductance plots are accompanied by color plots of the magnitude squared of the wavefunction at the Fermi energy, with low/moderate/high values corresponding to the usual blue/yellow/red color scheme. (This is the same wavefunction that determines the transmission coefficient. It involves many plane waves being injected with unit amplitude from the source lead into the structure's active region, as described in Section II.)

A. Zero Magnetic Field

The geometric potential defined in Section II-B is quite weak at the dimensions of our RQC, and its effect often goes undetected. At certain sheet electron densities N, however, it

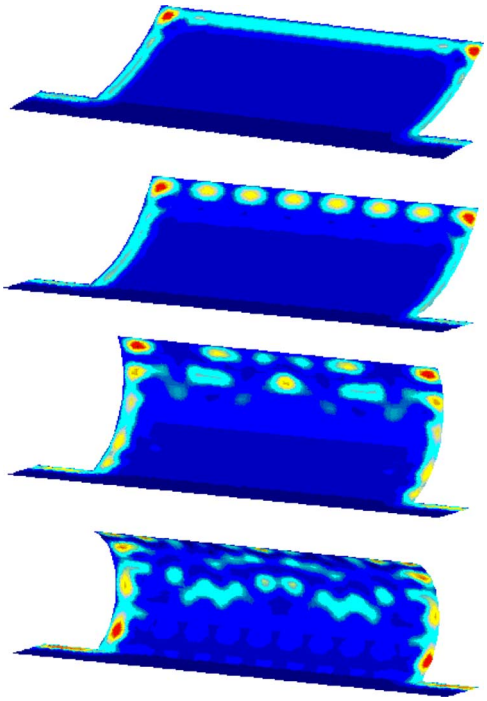

Fig. 5. Magnitude squared of the wavefunction at the Fermi energy in the nonplanar RQC as a function of curvature at a high magnetic field ($B = 12.5$ T). $N = 4 \times 10^{11}$ cm^{-2}. At low curvature ($\alpha = 0.4$, top panel) the edge state is clearly visible. As curvature increases ($\alpha = 0.5$, second panel), the edge state migrates away from the edge of the cavity and broadens. As the cavity takes on a distinctly cylindrical shape ($\alpha = 1.5$, third panel, and 1.7, bottom panel), it exhibits a midcavity state, created by opposing magnetic fluxes above and below it. Near wing of the cavity, where the probability density is effectively zero, has been removed so it would not obscure the images.

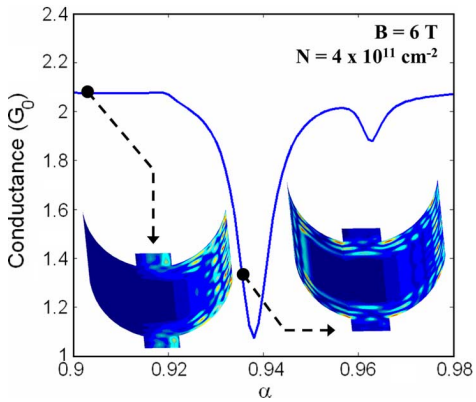

Fig. 6. Conductance variation with curvature at a high magnetic field ($B = 6$ T). Insets: colorized plots of the magnitude squared of the wavefunction at the Fermi energy, for the specific values of α shown. At certain magnetic fields, such as the one presented here, the cavity allows edge states which are prohibited in the narrow quantum-point contact. The shape of the cavity determines how these edge states couple to the modes in the contact; therefore, conductance again varies with curvature.

alone is responsible for significant variation in conductance. Hence, conductance can be modulated by changing the curvature even if in the absence of a magnetic field, as shown in Fig. 3. At lower curvatures, most of the plane waves incident from the source lead (top) are transmitted to the drain [note the high probability density in the drain-end quantum-point contact (right-hand-side inset)]. As the curvature increases, the coupling between the source and drain decreases, leading to a decrease in conductance.

B. Low Magnetic Field

At low magnetic fields, the resonance patterns which form in the cavity on account of the magnetic field [14], [15] can be altered by cavity curvature. These patterns determine the transmission through the cavity (see Fig. 4), and hence alter the conductance as well.

C. High Magnetic Field

At high magnetic fields, the results of our calculations confirm what is known about the physics of high-field magnetotransport in planar structures, such as the formation edge states and depopulation of Landau levels. In addition, novel effects of curvature on current conduction in the strong quantum Hall regime are also observed (see Fig. 5). At high fields, the edge states (top panel of Fig. 5) become wider and drift away from the edge of the cavity as the cavity rolls up (its curvature increases). As the cavity takes on a distinctly cylindrical shape, a midcavity state is formed as a result of opposing fluxes through the top and bottom portions of the wing.

At certain magnetic fields (Fig. 6), even minuscule changes in the curvature cause significant changes in the conductance. The conductance will remain sensitive to the changes in curvature in the high-field regime up to extremely high magnetic fields ($B > 8$ T in our particular example), after which the edge states become increasingly difficult to disturb by changes in curvature.

IV. Conclusion

We have developed a modified transfer-matrix method that enables low-bias, low-temperature transport calculations for nonplanar 2-D electron systems in the presence of magnetic fields. We have shown that the interplay between geometry and electronic properties of flexible SiGe/Si heterostructures (such as the simulated cylindrical resonant quantum cavity) is substantial. In particular, our results demonstrate that conductance through a cylindrical RQC at a given carrier density in the leads is highly sensitive to the changes in curvature for a wide range of magnetic field strengths, which suggests possible applications of nonplanar structures as nanoelectromechanical systems (NEMS) and sensors (e.g., a dilute chemical presence that affects the shape of the film could be detected electronically), at least at very low temperatures. At higher temperatures, scattering due to phonons must not be disregarded, and energies within a few k_BT around the Fermi level will contribute to the conductance, which may require including several Δ_2 subbands as well as some low-lying Δ_4 subbands. Consequently, smearing of the resonant features in G vs α (Figs. 3, 4, and 6) ought to be expected. Exploration of noncryogenic transport in nonplanar RQCs will be the topic of a subsequent publication.

References

[1] M. L. Leadbeater, C. L. Foden, J. H. Burroughes, M. Pepper, T. M. Burke, L. L. Wang, M. P. Grimshaw, and D. A. Ritchie, "Magneto-transport in a nonplanar two-dimensional electron gas," *Phys. Rev. B*, vol. 52, no. 12, pp. R8629–R8632, 1995.

[2] S. V. Golod, V. Y. Prinz, V. I. Mashanov, and A. K. Gutakovsy, "Fabrication of conducting GeSi/Si micro- and nanotubes and helical microcoils," *Semicond. Sci. Tech.*, vol. 16, pp. 181–185, 2001.

[3] H. Qin, N. Shaji, N. E. Merrill, H. S. Kim, R. C. Toonen, R. H. Blick, M. M. Roberts, D. E. Savage, M. G. Lagally, and G. Celler, "Formation of micro-tubes from strained SiGe/Si heterostructures," *New J. Phys.*, vol. 7, p. 241, 2005.
[4] M. M. Roberts, L. J. Klein, D. E. Savage, M. Friesen, G. K. Celler, M. A. Eriksson, and M. G. Lagally, "Elastically relaxed free-standing strained-Si nanomembranes," *Nature Mater.*, vol. 5, pp. 388–393, 2006.
[5] A. Lorke, S. Böhm, and W. Wegscheider, "Curved two-dimensional electron gases," *Superlattices Microstruct.*, vol. 33, pp. 347–356, 2003.
[6] S. Mendach, T. Kipp, H. Welsch, C. Heyn, and W. Hansen, "Interlocking mechanism for the fabrication of closed single-walled semiconductor microtubes," *Semicond. Sci. Tech.*, vol. 20, pp. 402–405, 2005.
[7] A. Chaplik, D. A. Romanov, and L. I. Magarill, "Ballistic transport in quantum cylinders," *Superlattices Microstruct.*, vol. 23, no. 6, pp. 1227–1230, 1998.
[8] L. I. Magarill and M. V. Entin, "Electrons in a curvilinear quantum wire," *J. Exp. Theor. Phys*, vol. 96, no. 4, pp. 766–774, 2003.
[9] C. Chryssomalakos, A. Franco, and A. Reyes-Coronado, "Spin-1/2 particle on a cylinder with radial magnetic field," *Eur. J. Phys*, vol. 25, pp. 489–502, 2004.
[10] A. Marchi, S. Reggiani, M. Rudan, and A. Bertoni, "Coherent electron transport in bent cylindrical surfaces," *Phys. Rev. B*, vol. 72, no. 035 403, pp. 1–10, 2005.
[11] T. Usuki, M. Saito, M. Takatsu, R. A. Kiehl, and N. Yokoyama, "Numerical analysis of ballistic-electron transport in magnetic fields by using a quantum point contact and a quantum wire," *Phys. Rev. B*, vol. 52, no. 11, pp. 8244–8255, 1995.
[12] T. Ando, "Quantum point contacts in magnetic fields," *Phys. Rev. B*, vol. 44, no. 15, pp. 8017–8027, 1991.
[13] W.-D. Sheng and L.-B. Xia, "A transfer matrix approach to conductance in quantum waveguides," *J. Phys., Condens. Matter*, vol. 8, pp. 3635–3645, 1996.
[14] R. Akis, D. K. Ferry, and J. P. Bird, "Magnetotransport fluctuations in regular semiconductor ballistic quantum dots," *Phys. Rev. B*, vol. 54, no. 24, pp. 705–715, 1996.
[15] S. Horie and A. Suzuki, "Mode coupling in ballistic quantum wires with double constrictions," *J. Phys. Soc. Jpn.*, vol. 71, no. 1, pp. 204–210, 2002.
[16] S. Goswami, K. A. Slinker, M. Friesen, L. M. McGuire, J. L. Truitt, C. Tahan, L. J. Klein, J. O. Chu, P. M. Mooney, D. W. van der Weide, R. Joynt, S. N. Coppersmith, and M. A. Eriksson, "Controllable valley splitting in silicon quantum devices," *Nature Phys.*, vol. 3, pp. 41–45, 2007.
[17] R. E. Peierls, "On the theory of the diamagnetism of conduction electrons," *Z. Phys.*, vol. 80, pp. 763–791, 1933.
[18] J. M. Luttinger, "The effect of a magnetic field on electrons in a periodic potential," *Phys. Rev.*, vol. 84, no. 4, pp. 814–817, 1951.
[19] W. Kohn, "Theory of Bloch electrons in a magnetic field: The effective Hamiltonian," *Phys Rev.*, vol. 115, no. 6, pp. 1460–1478, 1959.
[20] D. R. Hofstadter, "Energy levels and wave functions of Bloch electrons in rational and irrational magnetic fields," *Phys. Rev. B*, vol. 14, no. 6, pp. 2239–2249, 1976.
[21] R. C. T. DaCosta, "Quantum mechanics of a constrained particle," *Phys. Rev. A*, vol. 23, no. 4, pp. 1982–1987, 1981.

Gregory J. Meyer received the B.A. degree in biology from the University of Kansas, Lawrence, in 1993 and M.S. degree in electrical engineering from the University of Wisconsin, Madison, in 2006.

He is presently employed at Epic Healthcare Systems, Verona, WI.

Neville L. Dias received the B.E. degree in electronics and communications engineering from the Karnataka Regional Engineering College, Surathkal, India, in 2002. He is currently working toward the M.S. degree in electrical engineering at the University of Wisconsin, Madison.

His research interests include electronic transport in nanostructures and design of optoelectronic devices.

Robert H. Blick received the Ph.D. degree in physics from the Max-Planck-Institute for Solid State Research, Stuttgart, Germany in 1996.

He was a Research Fellow at the California Institute of Technology, Pasadena, after which he was an Assistant Professor at the University of Munich. In 2003 he joined the Electrical and Computer Engineering Department of the University of Wisconsin, Madison. In 2006 he was appointed to the Matthias Professorship in Engineering at the University of Wisconsin-Madison.

Irena Knezevic (S'02–M'04) received her Ph.D. degree in electrical engineering from Arizona State University, Tempe, AZ, in 2004.

In the Fall of 2004, she joined the faculty of the Electrical and Computer Engineering Department at the University of Wisconsin, Madison, as an Assistant Professor. Her research activities include quantum transport theory, simulation of electronic and optoelectronic devices, electronics properties of low-dimensional and curved nanostructures, and quantum information.

Dr. Knezevic is a member of the APS. She is a recipient of the 2004–2005 Palais' Oustanding Doctoral Student Award, as well as of the 2006 NSF Early Career Development (NSF CAREER) award.